energies

MDPI

Article

# Experimental Investigation on Performance of a Compression Ignition Engine Fueled with Waste Cooking Oil Biodiesel–Diesel Blend Enhanced with Iron-Doped Cerium Oxide Nanoparticles

**Meshack Hawi [1], Ahmed Elwardany [1,2], Mohamed Ismail [3] and Mahmoud Ahmed [1,4,*]**

1 Energy Resources Engineering Department, Egypt-Japan University of Science and Technology (E-JUST), New Borg El-Arab 21934, Egypt; meshack.ochieng@ejust.edu.eg (M.H.); ahmed.elwardany@ejust.edu.eg (A.E.)
2 Mechanical Engineering Department, Faculty of Engineering, Alexandria University, Alexandria 21544, Egypt
3 Mechanical Power Engineering Department, Faculty of Engineering, Zagazig University, Al-Sharkiah 44519, Egypt; manwar@zu.edu.eg
4 Mechanical Engineering Department, Assiut University, Faculty of Engineering, Assiut 71516, Egypt
* Correspondence: aminism@aun.edu.eg or Mahmoud.ahmed@ejust.edu.eg

Received: 14 January 2019; Accepted: 19 February 2019; Published: 27 February 2019


**Abstract:** The effect of iron-doped cerium oxide ($FeCeO_2$) nanoparticles as a fuel additive was experimentally investigated with waste cooking oil methyl ester (WCOME) in a four-stroke, single cylinder, direct injection diesel engine. The study aimed at the reduction of harmful emissions of diesel engines including oxides of nitrogen ($NO_x$) and soot. Two types of nanoparticles were used: cerium oxide doped with 10% iron and cerium oxide doped with 20% iron, to further investigate the influence of the doping level on the nanoparticle activity. The nanoparticles were dispersed in the tested fuels at a dosage of 90 ppm with the aid of an ultrasonic homogenizer. Tests were conducted at a constant engine speed of 2000 rpm and varying loads (from 0 to 12 N.m) with neat diesel (D100) and biodiesel–diesel blends of 30% WCOME and 70% diesel by volume (B30). The engine combustion, performance, and emission characteristics for the fuel blends with nanoparticles were compared with neat diesel as the base fuel. The test results showed improvement in the peak cylinder pressure by approximately 3.5% with addition of nanoparticles to the fuel. A reduction in $NO_x$ emissions by up to 15.7% were recorded, while there was no noticeable change in unburned hydrocarbon (HC) emissions. Carbon monoxide (CO) emission was reduced by up to 24.6% for B30 and 15.4% for B30 with nano-additives. Better engine performance was recorded for B30 with 20% $FeCeO_2$ as compared to 10% $FeCeO_2$, in regard to cylinder pressure and emissions. The brake specific fuel consumption was lower for the fuel blend of B30 with 10% $FeCeO_2$ nanoparticles, in low-to-medium loads and comparable to D100 at high loads. Hence, a higher brake thermal efficiency was recorded for the blend in low-to-medium loads compared to D100.

**Keywords:** waste cooking oil methyl ester; iron-doped cerium oxide nano-particles; diesel engine; combustion characteristics; emission characteristics

## 1. Introduction

For many decades, fossil fuels including petroleum, natural gas, and coal have been considered as the major energy resources globally. However, since these energy resources are non-renewable, they are likely to be depleted soon due to increasing demand resulting from rapid population growth

and industrialization. In addition, the excessive use of fossil fuels has led to negative implications for the environment. As a result, emission regulations are increasingly being strengthened to mitigate environmental degradation. Therefore, the need for cleaner and economically viable renewable energy sources has led researchers to seek new sources [1]. In this context, biodiesel produced from vegetable oils has been identified as a potential substitute for petroleum diesel in compression ignition engines [2].

Vegetable oils range from edible oils such as soybean, rapeseed, sunflower, palm [3], and coconut oil [4,5] to non-edible oils such as Karanja, Jatropha, Jojoba, Polanga, Mahua, rubber seed, cotton seed, tobacco, neem, linseed, and microalgae oil [6]. Other non-edible oils reported in the literature include eucalyptus oil, tea tree oil and, orange oil [7]. The use of non-edible oils as feedstock for biodiesel production has drawn greater research attention as it overcomes challenges related to food security and debate of food versus fuel. Furthermore, waste cooking oils are considered a cheaper biodiesel feedstock since the price of the oil is significantly lower compared with new oil from other sources [8]. An additional benefit associated with the use of waste cooking oil is that its recycling as an energy resource presents the best means of disposal.

Waste cooking oils have higher viscosity compared to conventional diesel fuel, and hence cannot be used directly in the diesel engine. The higher viscosity is caused by their larger molecular mass and chemical structure [9]. Transesterification process has been reported to be an effective method of viscosity reduction through the conversion of the waste cooking oil (WCO) to waste cooking oil methyl ester (WCOME) [10,11]. However, application of the resulting biodiesel in diesel engine leads to higher oxides of nitrogen ($NO_x$) emissions [12]. Experimental investigations by García-martín et al. [13] and Abu-Jrai et al. [14] reported notable increase in $NO_x$ emission with increasing quantities of waste cooking oil biodiesel in fuel blends with mineral diesel. Experimental measurements reported by Qasim et al. [15] on diesel engine operation with waste canola oil methyl esters also reveal higher $NO_x$ emission for biodiesel–diesel blends compared to neat diesel. Similar observations were made by Lin et al. [16] in an experimental study of diesel engine performance with normal diesel, biodiesel/diesel blends, and neat biodiesel derived from waste cooking oil from restaurants.

In an attempt to address the challenges of increased $NO_x$ emission from biodiesel-fueled compression ignition (CI) engines, recent studies have indicated that addition of certain nanoparticles to biodiesel has the potential to improve engine performance and lower exhaust emissions [17]. The nanomaterials most commonly considered as engine fuel additives include metal-based elements/compounds such as $Al_2O_3$, $CeO_2$, $TiO_2$, $FeCl_3$, MnO, ZnO, CuO, $Fe_3O_4$, Fe, Ce, Bo, and Al [18], as well as non-metal nano-materials such as graphite oxide (GO) and carbon nanotubes (CNTs) [19]. Ashok et al. [20] studied experimentally the effect of ZnO nanoparticles on combustion, performance, and emission characteristics of a twin cylinder CI engine operated with neat biodiesel fuel. They reported improvement in thermal efficiency by 4.7% and a reduction in $NO_x$ emission by 12.6% at full load. Related studies by Nanthagopal et al. [21] showed improved in-cylinder pressure and heat release rate with addition of ZnO and $TiO_2$ to biodiesel. A significant reduction in carbon monoxide (CO), unburned hydrocarbon (HC), and oxides of nitrogen ($NO_x$) emission were also reported.

Experimental investigations by Muthusamy et al. [22] on the effect of $Al_2O_3$ nanoparticles blended pongamia methyl ester on diesel engine performance showed marginal increase in brake thermal efficiency and significant reduction in CO, HC, and smoke emissions while $NO_x$ emission increased. Higher $NO_x$ emission with addition of $Al_2O_3$ nanoparticles was attributed to the combined effect of the oxygen content in biodiesel and the catalytic effect of nanoparticles. The enhanced combustion process generated elevated cylinder peak temperatures, hence oxidizing more nitrogen into nitric oxide. Improved diesel engine performance with addition of $Al_2O_3$ nanoparticles to Jatropha biodiesel [23] and Jojoba biodiesel [24] have also been reported.

A comprehensive experimental investigation was conducted by Selvan et al. [25] using Cerium Oxide ($CeO_2$) nanoparticles and carbon nanotubes as additives in Diesterol (diesel–biodiesel–ethanol) blends and significant improvement in engine performance was observed. The thermal efficiency

increased by up to 7.5%, while unburned hydrocarbon and smoke emission was reduced by 7.2% and 47.6%, respectively, relative to fuel blend without nanoparticles. This was attributed to cerium oxide nanoparticles acting as an oxygen donating catalyst which provides oxygen for the oxidation of carbon monoxide while absorbing oxygen, causing the reduction of oxides of nitrogen. It has been reported that cerium oxide also aids in burning off carbon deposits within the engine cylinder, hence reducing unburned hydrocarbon (UHC) and smoke emissions. Khalife et al. [26] studied diesel engine performance with emulsion fuel containing aqueous nano-$CeO_2$ additive in diesel–biodiesel blends and recorded improved combustion quality, where the brake specific fuel consumption (BSFC) was reduced by up to 16%, the brake thermal efficiency (BTE) improved by up to 23%, while CO, HC, and $NO_x$ emissions were reduced by 51%, 45%, and 27%, respectively.

Studies involving investigation on non-metal based nano-materials such as graphite oxide nanoparticles as fuel additives have been conducted with different fuels, including diesel [27,28] and biodiesel [29]. Carbon nanotubes have also been tested with diesohol (diesel + ethanol) [30], biodiesel [31,32], and water-diesel emulsion fuel [33]. Most of the studies have reported improved engine combustion, performance, and emission characteristics owing to the enhanced combustion process associated with the catalytic effect of the nano-additives.

More recent studies have focused on the use of a combination of different nanoparticles like cerium oxide (ceria)-zirconium dioxide nanoparticle ($CeO_2$-$ZrO_2$) [34], carbon nanotubes-ceria (CNT-ceria), and samarium-doped ceria (SDC) [35] as potential fuel additives for improved engine performance. Among oxides, ceria is considered one of the best hydrocarbon oxidation catalysts owing to the relative ease with which Ce can go from $Ce^{4+}$ to $Ce^{3+}$ [35]. Mirzajanzadeh et al. [36] reported a significant improvement in performance of a direct injection (DI) diesel engine fueled with diesel–biodiesel blends with addition of a hybrid nano-catalyst containing cerium oxide on amide-functionalized multiwall carbon nanotubes (MWCNT–$CeO_2$ catalyst). A significant overall improvement in engine performance was recorded for a fuel blend containing 20% biodiesel and 90 ppm of the catalyst. Engine torque and power improved by 4.91% and 7.89%, respectively, while $NO_x$, CO, HC, and soot was reduced by up to 18.9%, 38.8%, 71.4%, and 26.3%, respectively.

From the foregoing review, nano-additives have the potential for remarkable improvement of diesel engine performance with biodiesel and diesel–biodiesel fuel blends. It is also clearly seen that application of nanoparticles as additives in liquid fuel is an interesting concept which is yet to be fully explored. Therefore, the aim of the present study is to investigate the effect of iron-doped cerium oxide (Fe–$CeO_2$) on performance and emission characteristics of a CI engine fueled with biodiesel–diesel fuel blend. Several experimental investigations by different researchers have shown that cerium oxide nanoparticles have the potential to significantly improve engine performance and reduce exhaust emissions [25,36,37]. Furthermore, cerium oxide doped with certain elements such as iron has been reported to display higher catalytic activity compared to pure cerium oxide, in different applications [38]. Other studies have also reported a reduction in cerium oxide nanoparticles' size with increasing iron content, suggesting higher activity due to the larger surface area [39]. However, there is a scarcity of literature regarding the application of iron-doped cerium oxide in engine performance enhancement. The present study therefore seeks to investigate the performance of iron-doped cerium oxide as engine fuel additive.

From the literature, the optimum dosage of cerium oxide nanoparticles with biodiesel is reported as 90 ppm. Hence, in this research work, 90 ppm of iron-doped cerium oxide was added to biodiesel–diesel blend of 30% waste cooking oil methyl ester (denoted by B30) to investigate the combustion, performance, and emission characteristics of the diesel engine.

## 2. Materials and Methods

### *2.1. Nanoparticles Synthesis and Test Fuels Preparation*

A flame spray pyrolysis (FSP) process was implemented to synthesize Fe–$CeO_2$ nanoparticles. A detailed description of the experimental setup can be found in Reference [40]. Methane (purity 99.995%) was mixed with oxygen ($O_2$; purity 99.9995%), for the pilot flame; whereas oxygen at 8 bar was used as the dispersion gas in the spray nozzle for precursor atomization. Ferrocene (Sigma–Aldrich, St. Louis, MO, USA, 98%) dissolved in m-xylene (Sigma–Aldrich, 99%) was mixed with Ce (III) 2-ethylhexanoate (Sigma–Aldrich, 99% purity) and was used as the precursor for Fe–$CeO_2$ nanoparticles. Ferrocene was added to Ce (III) 2-ethylhexanoate with various concentrations to obtain Fe-doped $CeO_2$ nanoparticles with 10 and 20 atom % of iron with respect to the molar percentage of $CeO_2$. The precursor was injected using a syringe pump directly into the spray nozzle. Synthesized nanoparticles were collected on a glass-fiber filter with the aid of a vacuum pump. Figure 1a shows that doping iron in the $CeO_2$ nanoparticles changes the color from yellow to brown with and increase in the iron content. The iron-doped cerium oxide nanoparticles were subjected to X-ray diffraction (XRD) tests using X-Ray Diffractometer (XRD) (Shimadzu Xlab 6100, Kyoto, Japan) and the results on the variations of relative intensity with respect to diffraction angles are presented in Figure 1b. There was no change in the $CeO_2$ phase according to the National Institute of Standards and Technology (NIST) database [41], but the peaks were shifted to lower diffraction angles as the iron content increased.

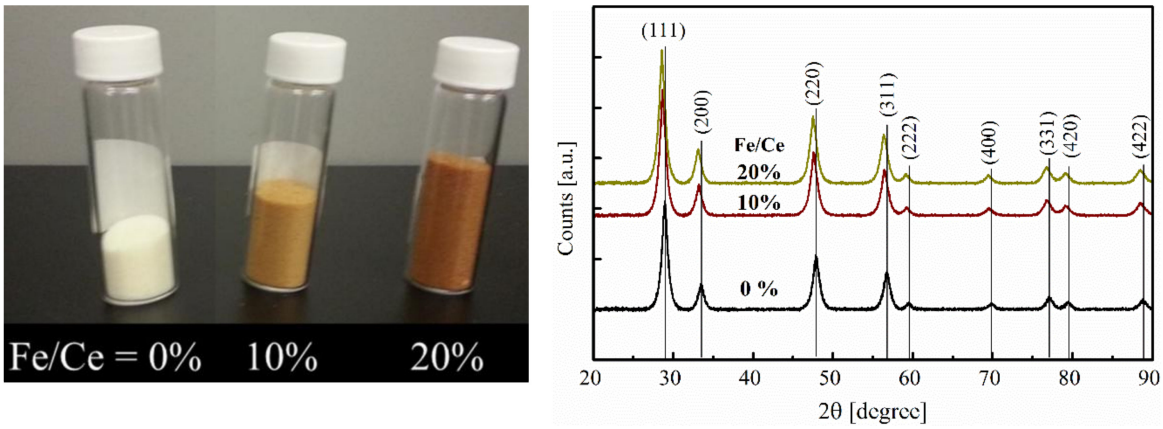


(**a**) (**b**)

**Figure 1.** (**a**) Direct images of pure and iron-doped cerium oxide nanoparticles; (**b**) XRD patterns of iron-doped cerium oxide nanoparticles (10% and 20%) compared to the pure cerium oxide nanoparticles (0%).

Photographic images of the nanoparticles obtained using the scanning electron microscope (SEM, JEOL JSM-6010LV, Tokyo, Japan) are shown in Figure 2a,b. The SEM micrographs show large clusters of particles with a porous nature commonly attributed to the synthesis process of cerium oxide nanoparticles [37]. Going deep into the images using a high resolution transmission electron microscope (HRTEM, JEOL JEM-2100F), as shown in Figure 2c,d, can illustrate the individual particles and their morphology. The average particle size is in the range of 5–7 nm with high crystallinity [42].

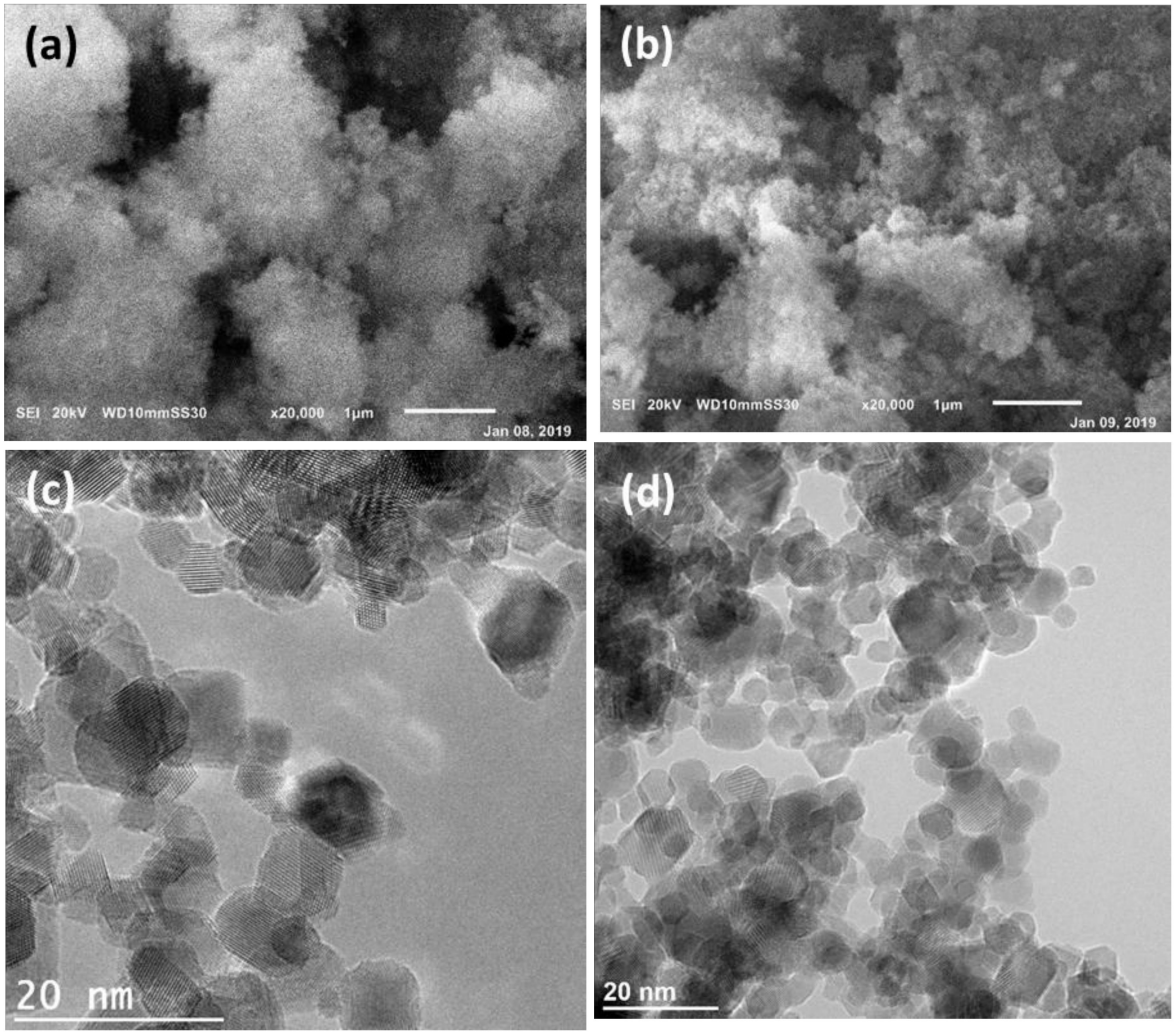


**Figure 2.** (**a**) SEM micrograph of iron-doped cerium oxide nanoparticles doped with 10% iron; (**b**) 20% iron; (**c**) HRTEM micrograph of iron-doped cerium oxide nanoparticles doped with 10% iron and (**d**) 20% iron.

The test fuels used in the experiments include diesel, diesel mixed with nanoparticles, a biodiesel–diesel blend, and a biodiesel–diesel blend with nanoparticles. The biodiesel–diesel fuel blend was prepared through mechanical agitation of a mixture of biodiesel and diesel, in the ratio of 30:70, while fuel mixtures with nanoparticles were prepared through ultra-sonication. In preparation of the nanoparticle-enhanced fuels, the iron-doped cerium oxide nanoparticles were added to the fuels at a 90-ppm concentration and mechanically agitated to form homogeneous fuel mixtures. The fuel mixtures were then kept in an ultrasonic homogenizer (UP400S, Hielscher Ultrasonics GmbH, Teltow, Germany) (UP400S: 400W, 24 kHz) for half an hour at 50% amplitude to improve mixture homogeneity and stability. The stability of the fuels with the addition of the nanoparticles was tested by monitoring samples of fuels mixed with nanoparticles, and no settling of the nanoparticles was noticed for a period of twenty-one days.

### *2.2. Experimental Setup*

A single cylinder diesel engine of power rating 5.5 kW at 3500 rpm connected to an asynchronous motor (Model TFCP 132SB-2) and equipped with the necessary instrumentation for engine performance evaluation was used in the experiments. Figure 3 shows a schematic representation of the engine experimental setup. More details about the experimental setup can be found in Reference [43]. The test rig (Model GUNT-CT100.22, Motorenfabrik Hatz GmbH & Co. KG, Ruhstorf, Germany) consisted of a

compression ignition (CI) engine of the technical specifications presented in Table 1. The asynchronous motor was used for starting the engine and for torque measurement.

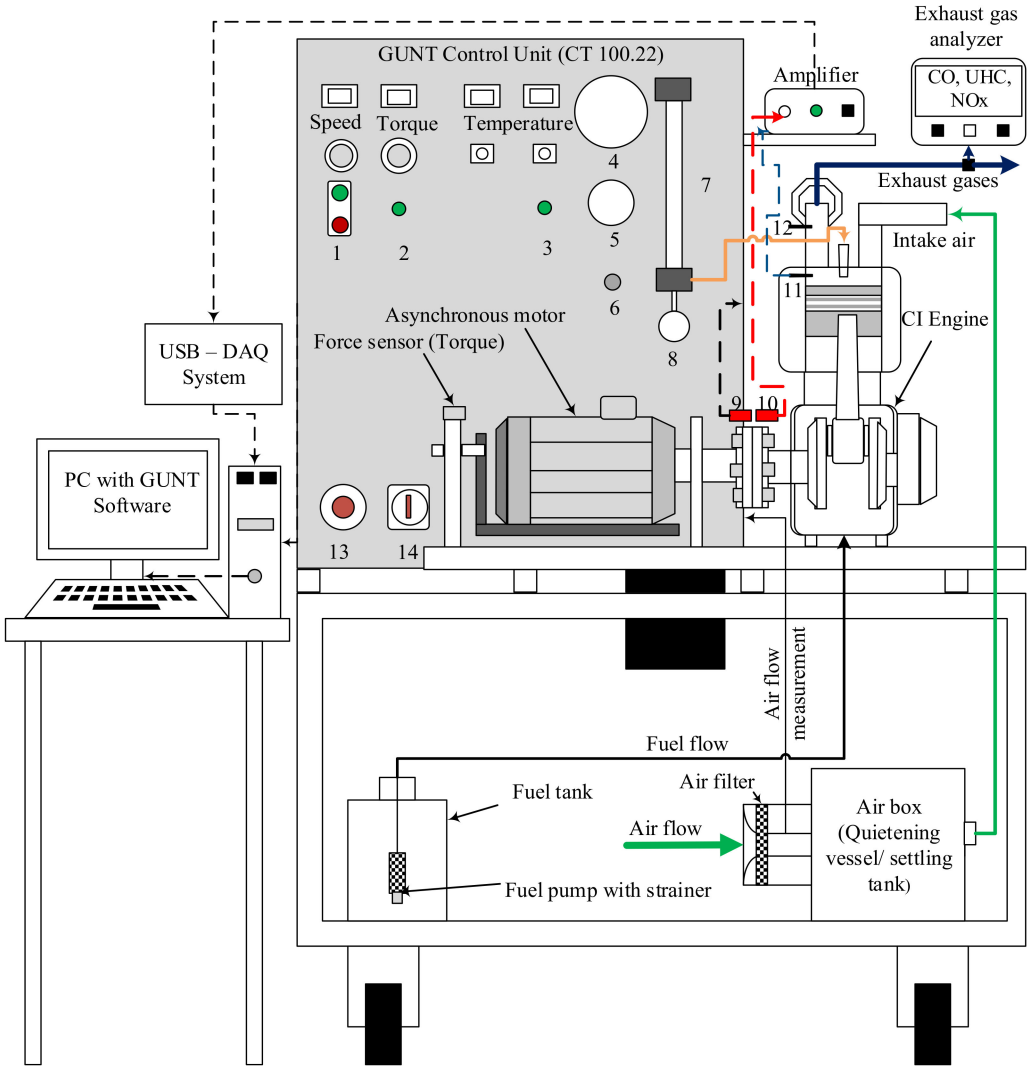


1 Electric motor switch, 2 Ignition switch, 3 Coolant pump switch, 4 Air consumption gauge, 5 Intake (negative) pressure gauge, 6 Fuel pump switch, 7 Fuel measuring tube, 8 Fuel consumption meter, 9 Speed sensor, 10 TDC sensor, 11 Kistler pressure transducer, 12 Exhaust gas temperature sensor, 13 Emergency switch, 14 Main switch.

**Figure 3.** Schematic of the engine experimental setup.

**Table 1.** Specifications of the test engine.

| Engine Parameter | Specification |
|---|---|
| Engine model | HATZ-1B30-2 |
| Engine type | Single cylinder 4-stroke direct injection compression ignition (CI) |
| Bore (mm) | 80 |
| Stroke (mm) | 69 |
| Crank length (mm) | 34.5 |
| Connecting rod length (mm) | 114.5 |
| Displacement volume ($cm^3$) | 347 |
| Compression ratio | 21.5:1 |
| Rated power (kW/rpm) | 5.5/3500 |
| Idle speed (rpm) | 1000 |
| Type of cooling | Air cooling |
| Start up | Electrical |

### 2.3. Experimental Procedure

All tests were conducted at a constant engine speed of 2000 rpm and varying engine load ranging from 0 to 12 N.m, at equal intervals of 3 N.m. Air and fuel consumption rates were measured by orifice meter (diameter of 20.6 mm) and flow meter sensor (Huba control type 680-out signal 0–10 volts diect current (VDC), Accuracy ±0.25% full scale (FS), respectively. Engine brake torque was measured by a force sensor of Model FLINTEC ZLB-200Kg-C3. Cylinder pressure was measured using a Kistler piezoelectric pressure sensor of Model 6052C connected to a charge amplifier (Model GUNT CT100.13), while the engine speed was measured through a proximity sensor (WACHENDORFF of type PNP-N. O, Sn 4 mm, 10-30VDC, and 200 mA). Rotation of the crank shaft was recorded by an optical encoder while a proximity switch of model WACHENDORFF PNP-N. O with a detecting distance of 4 mm was used to determine the position of the top dead center. A high speed data acquisition (DAQ) system (Model USB-AD16f) was used for the acquisition and analysis of cylinder pressure-crank angle data and signals from the force sensor, fuel flow meter sensor, air flow meter sensor, speed sensor, charge amplifier, and the proximity sensor. Three K-type thermocouples fixed at the intake port, exhaust port, and fuel line were used to measure the ambient air temperature, exhaust gas temperature, and fuel temperature, respectively. A desktop computer with LabVIEW software (GUNT software) was used for analyzing the data. Engine emissions were measured with ECA 450 exhaust gas analyzer. The exhaust gas sample was dried prior to analysis by passing it through a moisture trap to eliminate the water vapor. The gas sample was then passed through a filter to prevent particulates from entering the analyzer cell. Other technical specifications of the emission analyzer are given in Table 2. In-cylinder pressure data was recorded for fifty cycles and the average pressure calculated and used in determining the experimental heat release rate. Performance parameters including torque, engine speed, fuel flowrate, and air flowrate were recorded for forty cycles and the average values calculated for determination of performance characteristics such as BSFC and BTE.

**Table 2.** Specifications of the exhaust gas analyzer.

| Gas | Measuring Range | Resolution | Accuracy |
|---|---|---|---|
| CO | 0–4000 ppm | 1 ppm | ±5% of reading or ±10 ppm |
| $CO_2$ | 0–20% vol. | 0.1% vol. | ±0.5% of reading |
| HC | 0–10% vol. | 0.01% vol. | ±0.3% of reading |
| $O_2$ | 0–20.9% vol. | 0.01% vol. | ±0.3% of reading |
| $NO_x$ | 0–4000 ppm | 1 ppm | ±5% of reading or ±5 ppm |
| Stack temperature | −20 to 1315 °C | 1 °C | ±2 °C |
| Probe tip temperature | 800 °C max | - | - |

Experiments were conducted by first allowing the engine to warm up using normal diesel fuel until a constant exhaust temperature was achieved of around 120 ± 1 °C at 2000 rpm without engine loading. The fuel line was then switched to use the test fuel. The required engine torque was then set by adjusting the voltage to the asynchronous motor for a given engine speed. Finally, measurements were taken at steady state engine operation. The present study aims to investigate the influence of iron-doped cerium oxide nanoparticles on performance of CI engine with waste cooking oil methyl ester. Two types of nanoparticles were tested: cerium oxide doped with 10% iron (10% Fe + $CeO_2$) and cerium oxide doped with 20% iron (20% Fe + $CeO_2$), while fuel blending ratio was maintained as 30% biodiesel: 70% mineral diesel. The engine speed was kept constant at 2000 rpm while the engine load was varied according to the test plan shown in Table 3. After every test with biodiesel blend, the engine was run on pure diesel to clear the fuel system of any traces of the previously tested fuel.

**Table 3.** Experimental test program.

| Test Parameter | Range of Regulation | Analyzed Parameter |
|---|---|---|
| Fuel type | Neat diesel (D100), blended fuel (B30) | Cylinder pressure |
| Nanoparticle type | 10% Fe + $CeO_2$, 20% Fe + $CeO_2$ | BSFC and exhaust temperature, $T_{Exh}$ |
| Engine load (N.m) | 0, 3, 6, 9, and 12 | Emissions: CO, HC and NOx |
| Engine speed (rpm) | 2000 | |

### *2.4. Uncertainty Analysis*

The experimental uncertainties in the presented results were evaluated based on the root sum square method [44]. Table 4 gives the uncertainties of the various measuring devices used in the present study, as well as the percentage uncertainties of calculated parameters.

**Table 4.** Uncertainties of experimental measurements.

| Instrument | Range | Accuracy | Uncertainty |
|---|---|---|---|
| Torque indicator, N.m | 0–200 | ±1% of reading | 1 |
| Fuel burette, cc | 153 | ±0.2 | 1 |
| Speed sensor, rpm | 0–10,000 | ±5 rpm | 0.1 |
| Exhaust gas analyzer: | | | |
| CO, ppm | 0–4000 ppm | ±10 ppm | 1 |
| UHC, % vol. | 0–10 % vol. | ±0.3% of reading | 0.1 |
| $NO_x$, ppm | 0–4000 ppm | ±5 ppm | 1 |
| Pressure transducer, bar | 250 | ±1% of reading | 1 |
| Crank angle encoder, degree | 0–720 | ±0.5 | 0.3 |
| Brake power | - | - | ±1 |
| Brake specific fuel consumption (BSFC) | - | - | ±2 |
| Brake thermal efficiency (BTE) | - | - | ±3.2 |

### *2.5. Calculation of Experimental Heat Release Rate*

In this study, the experimental heat release rate is calculated using the first law-single zone model equation given by [45]:

$$\frac{dQ_{gross}}{d\theta} = \frac{\gamma(T)}{\gamma(T)-1} \times p\frac{dV}{d\theta} + \frac{1}{\gamma(T)-1} \times V\frac{dp}{d\theta} + \frac{dQ_{wall}}{d\theta} \quad (1)$$

where the ratio of specific heat, $\gamma(T)$ is calculated from:

$$\gamma(T) = 1.35 - 6 \times 10^{-5} \times T + 10^{-8} \times T^2 \quad (2)$$

where: $T$ is the mean temperature of in-cylinder gas.

The mean temperature of in-cylinder gases is obtained from the cylinder pressure and volume using the equation of state expressed in the form:

$$T = \frac{T_r p V}{p_r V_r} \quad (3)$$

The pressure, temperature and volume ($p_r$, $T_r$, and $V_r$, respectively) at the reference condition of intake valve closing IVC ($P_{IVC}$, $T_{IVC}$, $V_{IVC}$) are known. $T_{IVC}$ and $P_{IVC}$ are the temperature and the pressure at IVC, taken as 360 K and $1.013 \times 10^5$ Pa, respectively. The contents of the cylinder are assumed to behave as an ideal gas with the specific heat dependent on temperature [46]. The temperature and pressure of the combustion products are also assumed to be uniform at any moment during the combustion process.

Heat loss through the cylinder wall is evaluated from the convection heat transfer equation, as follows:

$$\frac{dQ_{wall}}{d\theta} = h_c A_{(\theta)}(T - T_{wall})\left(\frac{1}{6N}\right) \quad (4)$$

where the wall temperature, $T_{wall}$ is assumed as 470 K while the convection heat transfer coefficient, $h_c$ is estimated from Equation (5) [47]:

$$h_c = C_1 \times V^{-0.06} \times p^{0.8} \times T^{0.4} \times (C_2 + V_m)^{0.8} \quad (5)$$

where $p$ is the instantaneous pressure in bar, while $C_1$ and $C_2$ are constants ($C_1 = 130$ and $C_2 = 1.4$).

### *2.6. Properties of the Test Fuels*

Commercial mineral diesel and waste cooking oil methyl ester were used in the present study. The properties of the diesel and biodiesel fuels used are shown in Table 5.

**Table 5.** Properties of the test fuels [8].

| Property | Diesel | WCOME |
|---|---|---|
| Density@15.56 °C (kg/m$^3$) | 842.7 | 877 |
| Kinematic viscosity@40 °C (mm$^2$/s) | 3.34 | 4.9 |
| Calorific value (kJ/kg) | 45,448 | 37,951 |
| Boiling point (°C) | 180–360 | 250 |
| Flash point (°C) | 62 | 129 |
| Cetane number | 50 | 49 |
| Molecular weight (kg/kmol) | 191 | 305 |

## 3. Results and Discussion

This section presents the results on the effect of iron-doped cerium oxide nanoparticles on combustion, performance, and emissions characteristics of the CI engine fueled with diesel and biodiesel–diesel blend.

### *3.1. The Cylinder Pressure*

The variation of the cylinder pressure as a function of crank angle for an average of 50 successive cycles measured at engine speed of 2000 rpm and load of 12 N.m is shown in Figure 4. It was observed that the cylinder pressure was higher for the B30 fuel blend and for nano-additive enhanced fuels as compared to D100. It was also noticed that the pressure data was shifted to the left. This could be attributed to increased cetane number of the fuel and reduced ignition delay period with addition of nanoparticles [37].

Figure 5 shows the average cylinder pressure profile at a constant engine speed of 2000 rpm and varying engine loads. At a constant engine speed, the in-cylinder air motion as well as frictional losses of the engine remain the same, hence, any change in the in-cylinder pressure data could be attributed to either the change in the amount of injected fuel or fuel type. Generally, higher engine loads imply a larger amount of injected fuel. Hence, the peak cylinder pressure increases with engine load as can be seen in Figure 5a–e. It was also observed that the peak cylinder pressure increases with the addition of nanoparticles possibly due to enhanced combustion process. A greater improvement in cylinder pressure was observed at higher engine loads owing to enhanced combustion at higher temperatures.

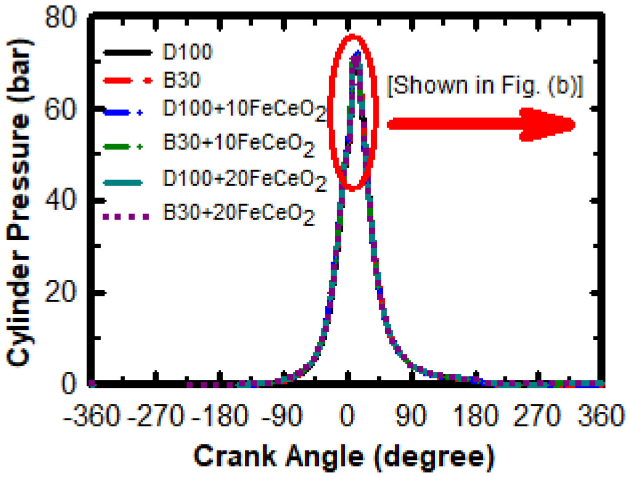


(**a**)

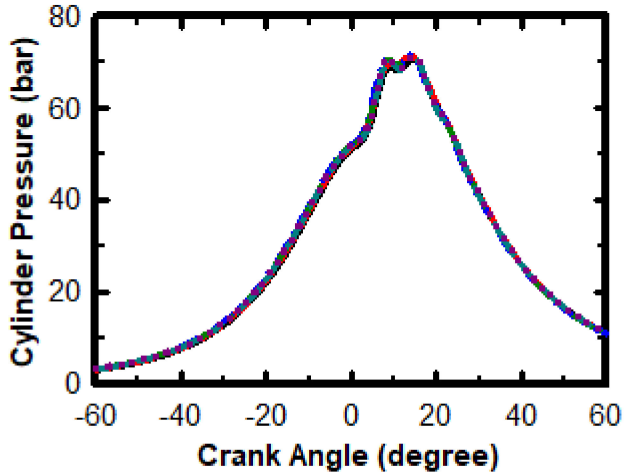


(**b**)

**Figure 4.** The average pressure ($P$) versus crank angle ($\theta$) for 50 successive cycles at engine speed of 2000 rpm and load of 12 N.m for different fuels: (**a**) the data during entire engine cycle and (**b**) the data during combustion.

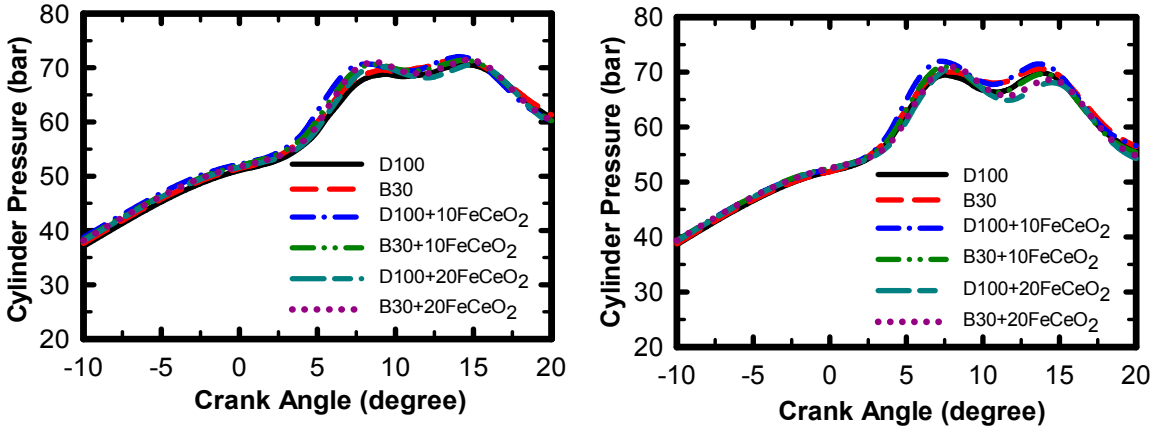


(**a**) (**b**)

**Figure 5.** *Cont.*

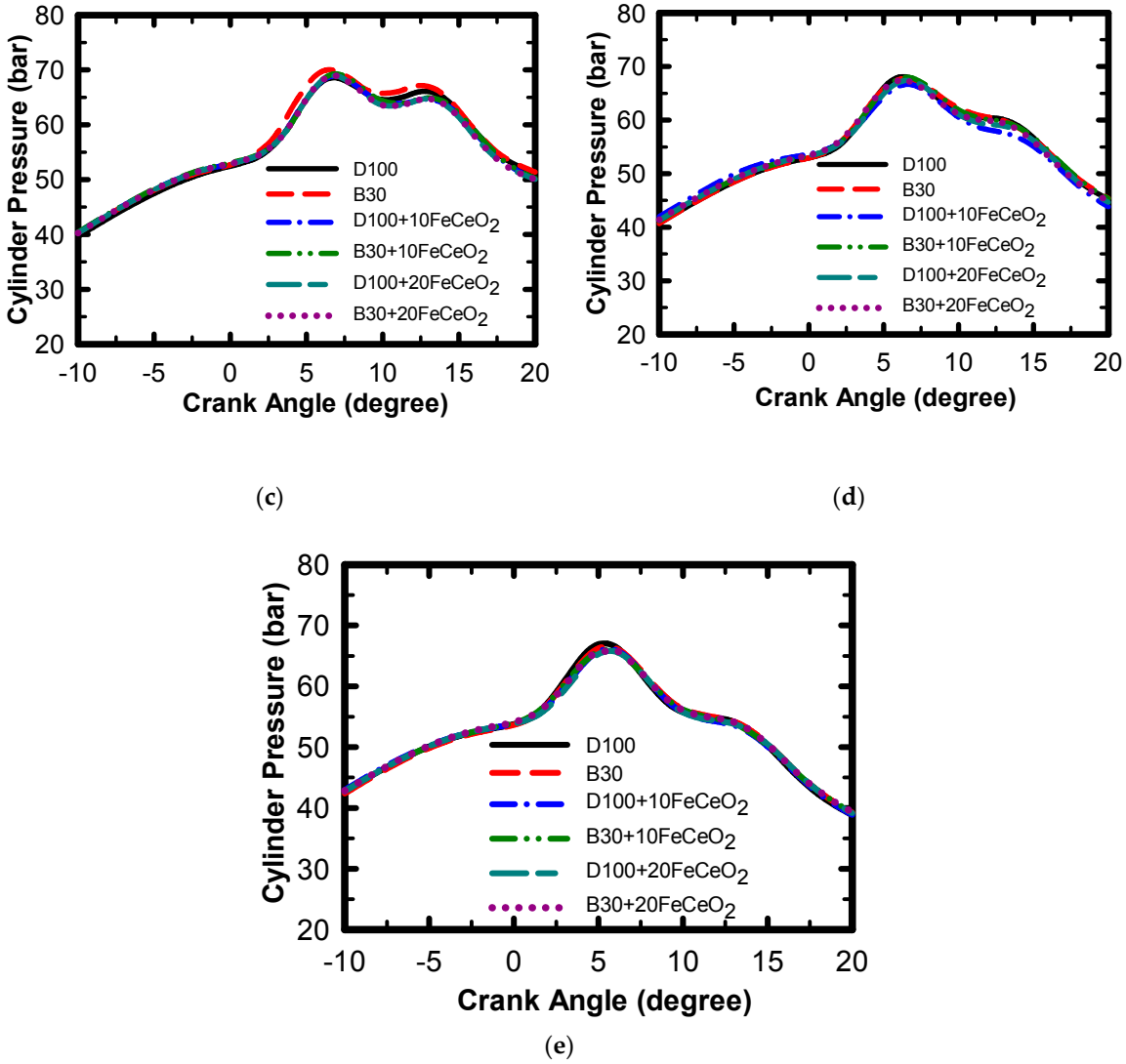


**Figure 5.** The average cylinder pressure profile at different engine loads and engine speed of 2000 rpm. (**a**) Engine load = 12 N.m; (**b**) Engine load = 9 N.m; (**c**) Engine load = 6 N.m; (**d**) Engine load = 3 N.m; (**e**) No engine load.

Figure 6a,b show the cylinder peak pressure ($P_{max}$) and the corresponding crank angle locations ($\theta_{Pmax}$), respectively. The cylinder peak pressure and its location are determined from the cylinder pressure profiles. From the figure, it can be observed that the peak pressure for B30 is comparable with that of D100 at all engine loads and it generally increases with addition of nanoparticles. The location of the peak cylinder pressure is delayed for higher engine loads, indicating that a greater amount of the injected fuel is burned during the diffusion combustion stage. Figure 6b shows that the fuel type has minimal effect on the location of the peak cylinder pressure.

The change in peak cylinder pressure for different fuel conditions relative to mineral diesel base fuel is shown in Figure 7. At low engine load, lower peak cylinder pressure is recorded for B30 and fuels with nanoparticles. However, at high engine loads, the peak cylinder pressure was higher for D100 by up to 3.5%, owing to an improved combustion process at higher engine loads.

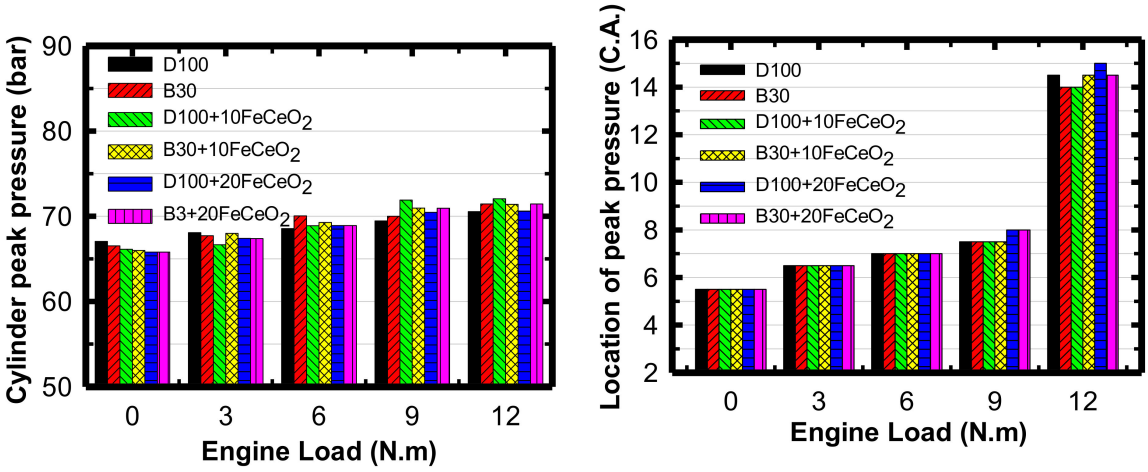


**Figure 6.** The peak cylinder pressure and its location at different engine loads for engine speed of 2000 rpm: (**a**) cylinder peak pressure (bar) and (**b**) location of the cylinder peak pressure (C.A.).

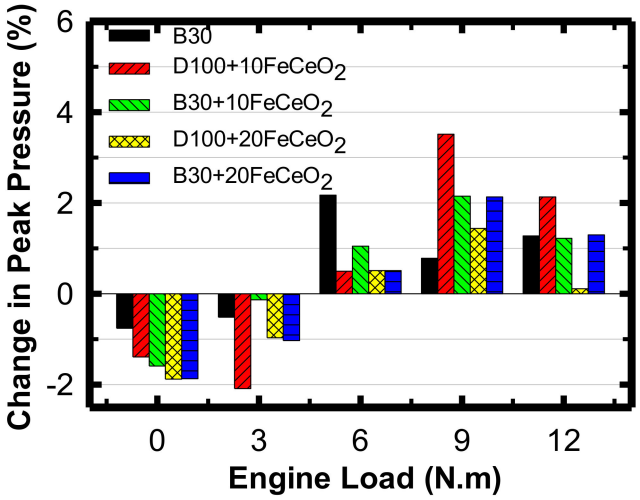


**Figure 7.** The change in cylinder peak pressure for different fuel conditions relative to mineral diesel base fuel (D100).

### *3.2. Engine Performance*

Engine performance parameters include quantities such as the BSFC of the BTE. Figure 8a–d shows the BSFC, BTE, fuel mass flow rate, and exhaust gas temperature ($T_{Exh}$) for engine operation at 2000 rpm with varying load and fuel conditions. For all the tested fuels, the BSFC reduced while the BTE improved with the increase in engine load. This could be attributed to the remarkable improvement in the fuel combustion quality at high engine load as seen in Figure 8a and b. It was also observed that the BSFC was lower for the fuel blend of B30 with 10 $FeCeO_2$ nanoparticles in low-to-medium loads and comparable to D100 at high loads. Consequently, the BTE for the blend was higher than that of D100 in low-to-medium loads and slightly lower at high loads. The improved BSFC and BTE of the fuel blend with nanoparticles could be attributed to enhanced combustion processes due to the catalytic effect of the nanoparticles [25]. The B30 fuel blend without nanoparticles shows higher BSFC and lower BTE compared to D100, possibly due to the lower calorific value of the biodiesel fuel, which implies that a larger quantity of the fuel was burned to generate equivalent power as D100 [8]. The trend for the fuel mass flow rate, as seen in Figure 8c shows a lower mass flow rate for B30 blend with 10 $FeCeO_2$ nanoparticles at low and medium loads, while the flow rate was comparable with D100 at high loads, indicating better fuel consumption with addition of nanoparticles. Figure 8d

shows minimal difference in the exhaust gas temperatures for different fuel conditions, except at high load where the nano-additive enhanced fuels show relatively lower exhaust temperatures.

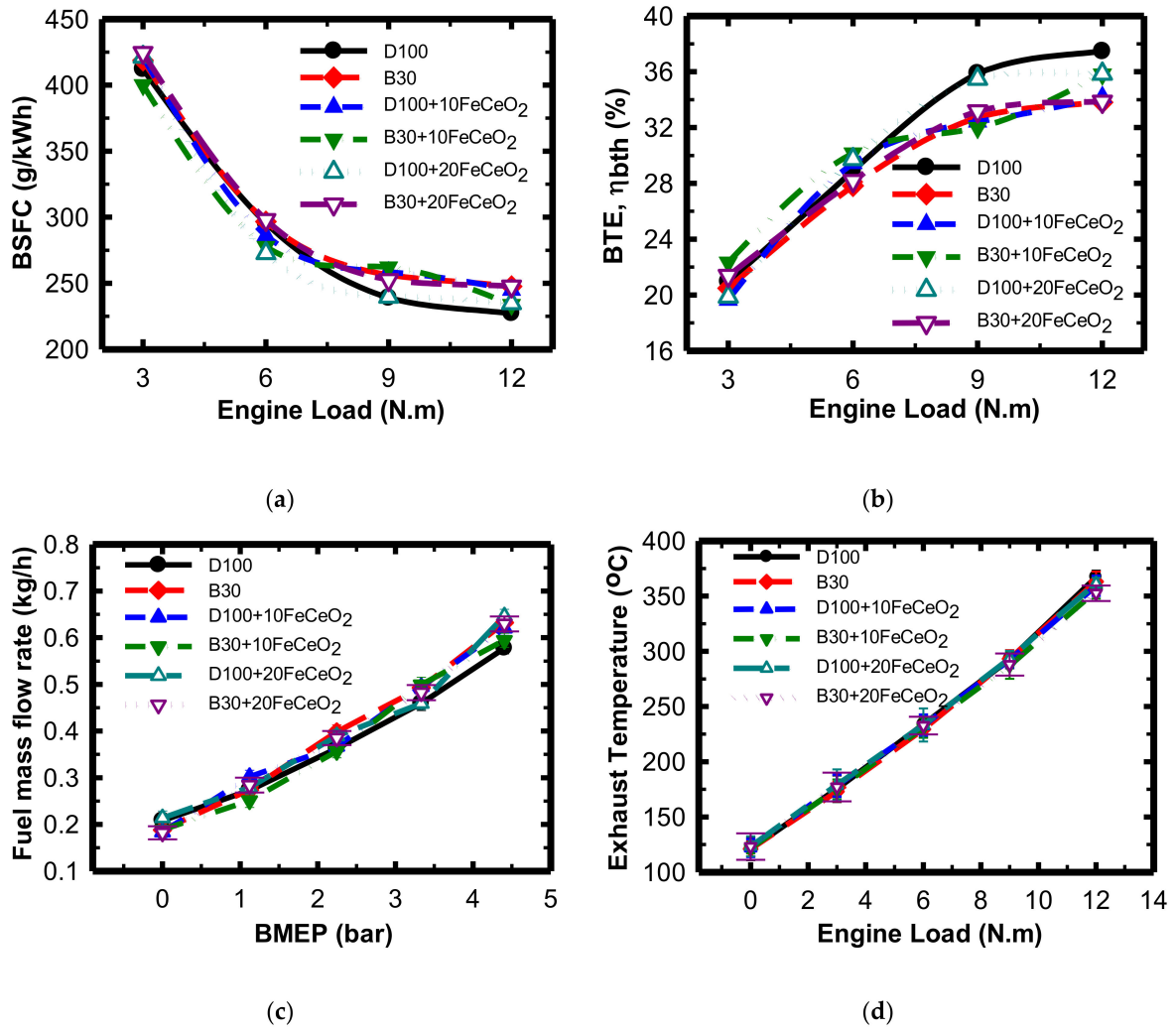


**Figure 8.** The variation of engine performance parameters with load at a speed of 2000 rpm: (**a**) BSFC; (**b**) BTE ($\eta_{bth}$); (**c**) fuel mass flow rate ($\dot{m}_{fuel}$); and (**d**) exhaust gas temperature, $T_{Exh}$.

### *3.3. Engine Emissions*

Figure 9a–d shows the engine emissions of $NO_x$ and CO, and the change in emission quantity for fuel blends relative to D100 at varying loads and a constant engine speed of 2000 rpm. The HC emissions were noticed to be unaffected by the fuel type or additive.

The variation of $NO_x$ emission with respect to engine load is shown in Figure 9a, while Figure 9b shows the relative change in NOx emission with reference to D100. Emissions of $NO_x$ from CI engines is formed from oxidation of atmospheric nitrogen, and is mainly thermal NO [48]. Increasing the engine load led to an increase in peak cycle temperature in the combustion chamber resulting in increased $NO_x$ emission for all the fuels. The fuel blend B30 had higher $NO_x$ emissions compared to all the other fuels due to the extra oxygen atom in the biodiesel structure which enhanced the combustion rate, contributing to increased peak cycle temperature and consequently higher thermal $NO_x$ formation [37,49,50]. The B30 fuel blend with nanoparticles had lower $NO_x$ compared to all the other fuels since the nanoparticle acts as a reducing agent which converts oxides of nitrogen to nitrogen and oxygen, leading to significant reduction in $NO_x$. Cerium oxide ($CeO_2$) reacts with hydrocarbon to form cerous oxide ($Ce_2O_3$), water vapour ($H_2O$), and $CO_2$ according to Equation (6). The reduction

reaction then occurs as shown in Equation (7), due to the high thermal stability of the cerous oxide, shown in Equation (8) [25,37].

$$(2y + x)CeO_2 + H_xC_y \rightarrow [(2y + x)/2]Ce_2O_3 + x/2H_2O + y/2CO_2 \quad (6)$$

$$Ce_2O_3 + NO \rightarrow 2CeO_2 + 1/2N_2 \quad (7)$$

$$2CeO_2 \leftrightarrow Ce_2O_3 + 1/2O_2 \quad (8)$$

Several authors reported the same trend with addition of cerium oxide nanoparticles to diesel and diesel blends with biodiesel from different sources [25,37,51]. The cerium oxide nanoparticles act as catalyst for the combustion reaction by providing oxygen for the oxidation of hydrocarbons and soot, hence higher cylinder peak pressure. However, lower $NO_x$ emission was recorded, indicating that part of the NO produced reacts with the nanoparticles and was reduced to nitrogen.

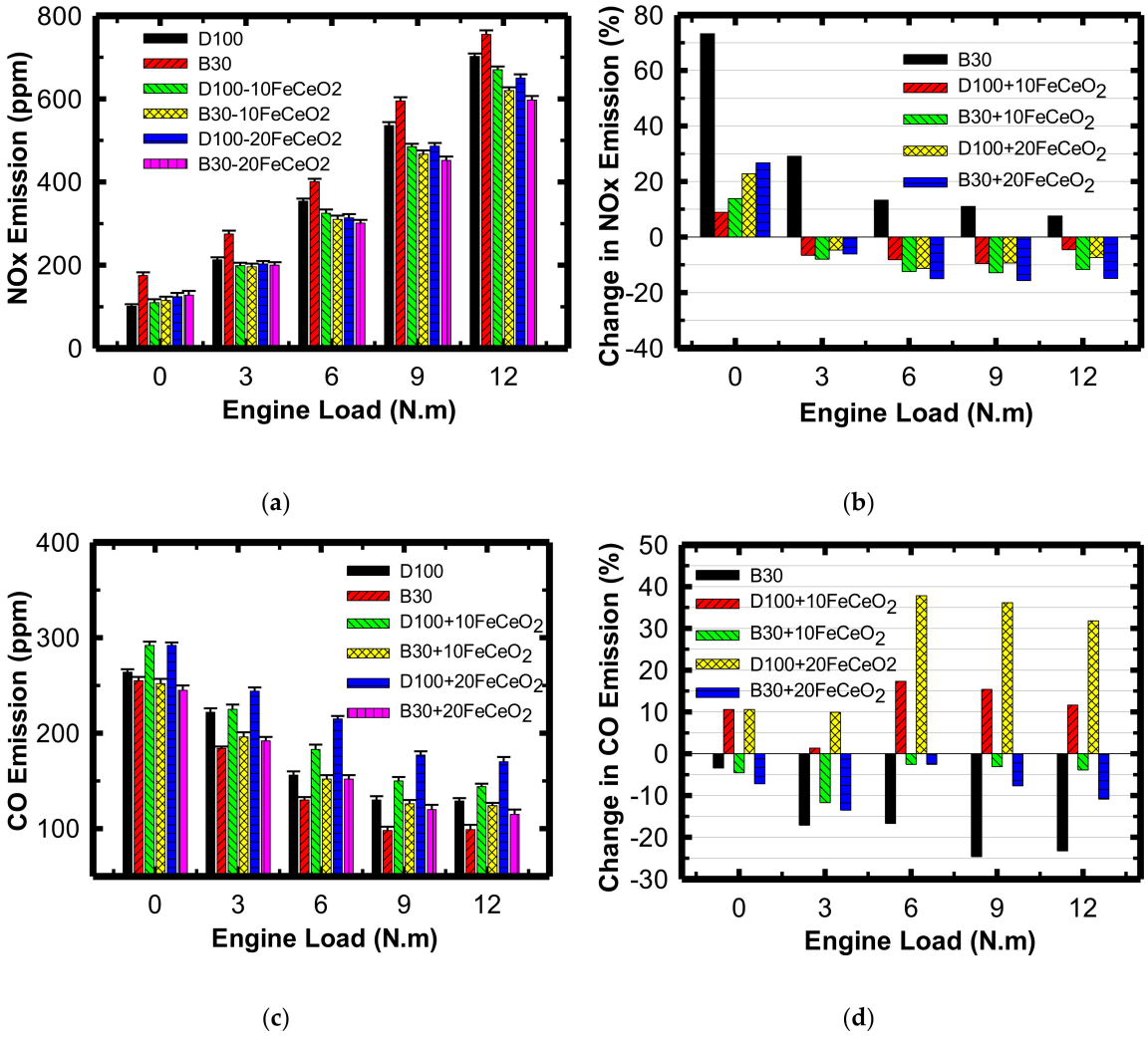


**Figure 9.** The engine emissions at different loads for different fuels at a speed of 2000 rpm: (**a**) $NO_x$ emission, (**b**) change in NOx emission relative to D100, (**c**) CO emission, and (**d**) change in CO emission relative to D100.

The maximum reduction in $NO_x$ emission of 15.7 % was recorded for B30 fuel blend with cerium oxide doped with 20% iron. Aneggi et al. [34] studied experimentally the effect of different ceria-based catalysts including pure ceria, zirconium-doped ceria, and iron-doped ceria on the combustion of diesel soot. They reported that iron-doped ceria showed the highest activity. The higher activity of

the Fe-modified ceria catalysts was attributed mainly to the oxygen storage/redox capacity and large surface area of the catalyst. Related studies have reported a decrease in particle size with iron doping concentration, implying higher activity with increasing iron concentration [39].

Figure 9c–d show the variation of CO emission with engine load and the relative change in CO emission with reference to D100, respectively. The quantity of CO emission decreases as the engine load increases due to higher combustion temperatures which enhances the oxidation of more CO to $CO_2$. It was also observed that CO emissions were lowest for B30 at all loading conditions, possibly due to the extra oxygen provided by the biodiesel, which promotes the complete oxidation of CO to $CO_2$. Addition of nanoparticles to the fuel blends was noted to increase slightly the CO emissions. However, addition of the iron-doped cerium oxide nanoparticles to B30 yields a net reduction in CO emissions of up to 24.6% with reference to neat diesel.

## 4. Conclusions

The combustion, performance, and emission characteristics of a four-stroke single cylinder diesel engine with nano-additive enhanced diesel and biodiesel–diesel blends were investigated to understand the effects of iron-doped cerium oxide nanoparticles as a fuel additive in diesel and diesel–WCOME blends. Based on the experimental results, the following conclusions are drawn:

1. The addition of iron-doped cerium oxide nanoparticles in a biodiesel–diesel blend increases the cylinder gas pressure as the nanoparticles enhanced the combustion process. However, the variation between the fuel mixtures containing cerium oxide doped with 10% iron and cerium oxide doped with 20% iron was marginal.
2. The cylinder peak pressure increased by up to 3.5% with the addition of nanoparticles to the B30 fuel blend due to enhanced combustion processes by the nanoparticles.
3. $NO_x$ emission for the B30 blend was reduced by up to 15.7% with the addition of iron-doped cerium oxide nanoparticles.
4. Addition of nanoparticles to the D100 and B30 fuels had no noticeable effect on HC emissions.
5. CO emissions were reduced by up to 24.6% for B30 and 15.4% for B30 with nano-additives, relative to D100.
6. Better engine performance was recorded for B30 with 20% $FeCeO_2$ as compared to 10% $FeCeO_2$, regarding cylinder pressure and emissions. Additionally, the fuel blend B30 with 10% $FeCeO_2$ nanoparticles recorded better BSFC and BTE in low-to-medium loads compared to D100.

**Author Contributions:** All authors contributed equally to this work.

**Acknowledgments:** The authors gratefully acknowledge the financial support from Japan International Corporation Agency (JICA) and Egypt–Japan University of Science and Technology (E–JUST) in acquiring the materials, equipment, and facilities used in this study.

**Conflicts of Interest:** The authors declare no conflict of interest.

## Nomenclature

***Abbreviations***

| | |
|---|---|
| WCOME | waste cooking oil methyl ester |
| WCO | waste cooking oil |
| CI | compression ignition |
| IC | internal combustion |
| $NO_x$ | oxides of nitrogen |
| HC | unburned hydrocarbon |
| CO | carbon monoxide |
| PM | particulate matter |
| GO | graphite oxide |
| BSFC | brake specific fuel consumption |

| | |
|---|---|
| BTE | brake thermal efficiency |
| C.A. | crank angle |
| CNTs | carbon nanotubes |
| MWCNTs | multiwall carbon nanotubes |
| SDC | samarium-doped ceria |
| IVC | intake valve closing |
| *Symbols* | |
| $\gamma$ | specific heat ratio |
| $\theta$ | crank angle |
| $p$ | instantaneous cylinder pressure (bar) |
| $T$ | mean gas temperature (K) |
| $V$ | cylinder volume ($m^3$) |
| $V_r$, $T_r$, $P_r$ | volume, temperature and pressure at any reference condition |
| $\eta_{bth}$ | brake thermal efficiency |
| $\dot{m}_{fuel}$ | fuel mass flow rate |
| *Subscripts* | |
| T | temperature |
| *r* | reference condition |
| max | maximum |
| *Exh* | exhaust |
| *bth* | brake thermal |

## References


1. Tesfa, B.; Gu, F.; Mishra, R.; Ball, A. Emission characteristics of a CI engine running with a range of biodiesel feedstocks. *Energies* **2014**, *7*, 334–350. [CrossRef]
2. Gui, M.M.; Lee, K.T.Ã.; Bhatia, S. Feasibility of edible oil vs. non-edible oil vs. waste edible oil as biodiesel feedstock. *Energy* **2008**, *33*, 1646–1653. [CrossRef]
3. Kim, H.Y.; Ge, J.C.; Choi, N.J. Application of palm oil biodiesel blends under idle operating conditions in a common-rail direct-injection diesel engine. *Appl. Sci.* **2018**, *8*, 2665. [CrossRef]
4. Agarwal, A.K.; Gupta, J.G.; Dhar, A. Potential and challenges for large-scale application of biodiesel in automotive sector. *Prog. Energy Combust. Sci.* **2017**, *61*, 113–149. [CrossRef]
5. Mattarelli, E.; Rinaldini, C.A.; Savioli, T. Combustion analysis of a diesel engine running on different biodiesel blends. *Energies* **2015**, *8*, 3047–3057. [CrossRef]
6. Ashraful, A.M.; Masjuki, H.H.; Kalam, M.A.; Fattah, I.R.; Imtenan, S.; Shahir, S.A.; Mobarak, H.M. Production and comparison of fuel properties, engine performance, and emission characteristics of biodiesel from various non-edible vegetable oils: A review. *Energy Convers. Manag.* **2014**, *80*, 202–228. [CrossRef]
7. Rahman, S.M.; Nabi, M.; Van, T.; Suara, K.; Jafari, M.; Dowell, A.; Islam, M.; Marchese, A.; Tryner, J.; Hossain, M.; et al. Performance and combustion characteristics analysis of multi-cylinder CI engine using essential oil blends. *Energies* **2018**, *11*, 738. [CrossRef]
8. Attia, A.M.A.; Hassaneen, A.E. Influence of diesel fuel blended with biodiesel produced from waste cooking oil on diesel engine performance. *Fuel* **2016**, *167*, 316–328. [CrossRef]
9. Karmakar, A.; Karmakar, S.; Mukherjee, S. Properties of various plants and animals feedstocks for biodiesel production. *Bioresour. Technol.* **2010**, *101*, 7201–7210. [CrossRef] [PubMed]
10. Atapour, M.; Kariminia, H.; Moslehabadi, P.M. Optimization of biodiesel production by alkali-catalyzed transesterification of used frying oil. *Process Saf. Environ. Prot.* **2014**, *92*, 179–185. [CrossRef]
11. Keera, S.T.; Sabagh SMEl Taman, A.R. Transesterification of vegetable oil to biodiesel fuel using alkaline catalyst. *Fuel* **2011**, *90*, 42–47. [CrossRef]
12. Kathirvel, S.; Layek, A.; Muthuraman, S. Exploration of waste cooking oil methyl esters (WCOME) as fuel in compression ignition engines: A critical review. *Eng. Sci. Technol. Int. J.* **2016**, *19*, 1018–1026. [CrossRef]
13. García-Martín, J.F.; Barrios, C.C.; Dominguez-Sáez, A.; Alvarez-Mateos, P. Biodiesel production from waste cooking oil in an oscillatory flow reactor. Performance as a fuel on a TDI diesel engine. *Renew. Energy* **2018**, *125*, 546–556. [CrossRef]

14. Abu-Jrai, A.; Yamin, J.A.; Al-muhtaseb, A.H.; Hararah, M.A. Combustion characteristics and engine emissions of a diesel engine fueled with diesel and treated waste cooking oil blends. *Chem. Eng. J.* **2011**, *172*, 129–136. [CrossRef]
15. Qasim, M.; Ansari, T.M.; Hussain, M. Combustion, performance, and emission evaluation of a diesel engine with biodiesel like fuel blends derived from a mixture of Pakistani waste canola and waste transformer oils. *Energies* **2017**, *10*, 1023. [CrossRef]
16. Lin, Y.; Wu, Y.G. Combustion characteristics of waste-oil produced biodiesel/diesel fuel blends. *Fuel* **2007**, *86*, 1772–1780. [CrossRef]
17. Ali, O.M.; Mamat, R.; Faizal, C.K.M.; Ali, O.M.; Mamat, R.; Faizal, C.K.M. Review of the effects of additives on biodiesel properties, performance, and emission features. *J. Renew. Sustain. Energy* **2013**, *5*. [CrossRef]
18. Saxena, V.; Kumar, N.; Kumar, V. A comprehensive review on combustion and stability aspects of metal nanoparticles and its additive effect on diesel and biodiesel fuelled C.I. engine. *Renew. Sustain. Energy Rev.* **2017**, *70*, 563–588. [CrossRef]
19. Khalife, E.; Tabatabaei, M.; Demirbas, A.; Aghbashlo, M. Impacts of additives on performance and emission characteristics of diesel engines during steady state operation. *Prog. Energy Combust. Sci.* **2017**, *59*, 32–78. [CrossRef]
20. Ashok, B.; Nanthagopal, K.; Mohan, A.; Johny, A.; Tamilarasu, A. Comparative analysis on the effect of Zinc Oxide and Ethanox as additives with biodiesel in CI engine. *Energy* **2017**, *140*, 352–364. [CrossRef]
21. Nanthagopal, K.; Ashok, B.; Tamilarasu, A.; Johny, A.; Mohan, A. Influence on the effect of zinc oxide and titanium dioxide nanoparticles as an additive with Calophyllum inophyllum methyl ester in a CI engine. *Energy Convers. Manag.* **2017**, *146*, 8–19. [CrossRef]
22. Muthusamy, S.; Nallathambi, S.S.; Ramasamy, R.; Thasthagir, S.; Hussain, M. Effect of aluminium oxide nanoparticles blended pongamia methyl ester on performance, combustion and emission characteristics of diesel engine. *Renew. Energy* **2018**, *116*, 518–526. [CrossRef]
23. Patel, H.K.; Kumar, S. Experimental analysis on performance of diesel engine using mixture of diesel and bio-diesel as a working fuel with Aluminum Oxide nanoparticle additive. *Therm. Sci. Eng. Prog.* **2017**, *4*, 252–258. [CrossRef]
24. Attia, A.M.A.; El-Seesy, A.I.; El-Batsh, H.M.; Shehata, M.S. Effects of alumina nanoparticles additives into jojoba methyl ester-diesel mixture on diesel engine performance. In Proceedings of the ASME 2014 International Mechanical Engineering Congress and Exposition, IMECE2014, Montreal, QC, Canada, 14–20 November 2014; pp. 1–10.
25. Selvan, V.A.M.; Anand, R.B.; Udayakumar, M. Effect of cerium oxide nanoparticles and carbon nanotubes as fuel-borne additives in diesterol blends on the performance, combustion and emission characteristics of a variable compression ratio engine. *Fuel* **2014**, *130*, 160–167. [CrossRef]
26. Khalife, E.; Tabatabaei, M.; Najafi, B.; Mostafa, S. A novel emulsion fuel containing aqueous nano cerium oxide additive in diesel-biodiesel blends to improve diesel engines performance and reduce exhaust emissions: Part I-Experimental analysis. *Fuel* **2017**, *207*, 741–750. [CrossRef]
27. Ooi, J.B.; Ismail, H.M.; Swamy, V.; Wang, X.; Swain, A.K.; Rajanren, J.R. Graphite oxide nanoparticles as diesel fuel additive for cleaner emissions and lower fuel consumption. *Energy Fuels* **2016**, *30*, 1341–1353. [CrossRef]
28. Ooi, J.B.; Ismail, H.M.; Tan, B.T.; Wang, X. Effects of Graphite Oxide and single-walled carbon nanotubes as diesel additives on the performance, combustion, and Emission characteristics of a light-duty diesel engine. *Energy* **2018**, *161*, 70–80. [CrossRef]
29. Boon, J.; Jeevan, O.; Rajanren, R.; Mohamed, H. Improving combustion characteristics of diesel and biodiesel droplets by graphite oxide addition for diesel engine applications. *Int. J. Energy Res.* **2017**, *41*, 1–10. [CrossRef]
30. Heydari-maleney, K.; Taghizadeh-alisaraei, A.; Ghobadian, B.; Abbaszadeh-mayvan, A. Analyzing and evaluation of carbon nanotubes additives to diesohol-B2 fuels on performance and emission of diesel engines. *Fuel* **2017**, *196*, 110–123. [CrossRef]
31. Balaji, G.; Cheralathan, M. Effect of CNT as additive with biodiesel on the performance and emission characteristics of a DI diesel engine. *Int. J. ChemTech Res.* **2015**, *7*, 1230–1236.

32. Ghafoori, M.; Ghobadian, B.; Najafi, G.; Layeghi, M.; Rashidi, A.; Mamat, R. Effect of nano-particles on the performance and emission of a diesel engine using biodiesel-diesel blend. *Int. J. Automot. Mech. Eng.* **2015**, *12*, 3097–3108. [CrossRef]
33. Basha, J.S.; Anand, R.B. An experimental investigation in a diesel engine using carbon nanotubes blended water-diesel emulsion fuel. *Proc. Inst. Mech. Eng. Part A J. Power Energy* **2011**, *225*, 279–288. [CrossRef]
34. Aneggi, E.; De Leitenburg, C.; Dolcetti, G.; Trovarelli, A. Promotional effect of rare earths and transition metals in the combustion of diesel soot over CeO2 and CeO2-ZrO2. *Catal. Today* **2006**, *114*, 40–47. [CrossRef]
35. Zhao, S.; Gorte, R.J. A comparison of ceria and Sm-doped ceria for hydrocarbon oxidation reactions. *Appl. Catal.* **2004**, *277*, 129–136. [CrossRef]
36. Mirzajanzadeh, M.; Tabatabaei, M.; Ardjmand, M.; Rashidi, A. A novel soluble nano-catalysts in diesel-biodiesel fuel blends to improve diesel engines performance and reduce exhaust emissions. *Fuel* **2015**, *139*, 374–382. [CrossRef]
37. Annamalai, M.; Dhinesh, B.; Nanthagopal, K.; SivaramaKrishnan, P.; Lalvani, J.I.; Parthasarathy, M.; Annamalai, K. An assessment on performance, combustion and emission behavior of a diesel engine powered by ceria nanoparticle blended emulsified biofuel. *Energy Convers. Manag.* **2016**, *123*, 372–380. [CrossRef]
38. Channei, D.; Wetchakun, N.; Siriwong, C.; Phanichphant, S. Synthesis and characterization of Fe-doped $CeO_2$ nanoparticles and their photocatalytic activities. In Proceedings of the 2010 5th IEEE International Conference on Nano/Micro Engineered and Molecular Systems, Xiamen, China, 20–23 January 2010; pp. 43–48.
39. Dhannia, T.; Jayalekshmi, S.; Kumar, M.C.S.; Rao, T.P.; Bose, A.C. Effect of iron doping and annealing on structural and optical properties of cerium oxide nanocrystals. *J. Phys. Chem. Solids* **2010**, *71*, 1020–1025. [CrossRef]
40. Ismail, M.A. Combustion Synthesis of Nanomaterials Using Various Flame Configurations. Ph.D. Thesis, King Abdullah University of Science and Technology (KAUST), Thuwal, Saudi Arabia, 2016.
41. McCullough, J.D. An X-Ray Study of the Rare-Earth Oxide Systems: CeIV-NdIII, CeIV-PrIII, CeIV-PrIV, and PrIV-NdIII. *J. Am. Chem. Soc.* **1950**, *72*, 1386. [CrossRef]
42. Ismail, M.A.; Memon, N.K.; Hedhili, M.N.; Anjum, D.H.; Chung, S.H. Synthesis of $TiO_2$ nanoparticles containing Fe, Si, and V using multiple diffusion flames and catalytic oxidation capability of carbon-coated nanoparticles. *J. Nanopart. Res.* **2016**, *18*, 1–14. [CrossRef]
43. El-seesy, A.I.; Abdel-rahman, A.K.; Hassan, H.; Ookawara, S.; Hawi, M. Biodiesel-diesel fuel mixture with addition of nanoparticles. In Proceedings of the ASME 2017 Power Conference Joint with ICOPE-17, Charlotte, NC, USA, 26–30 June 2017; pp. 1–9.
44. Coleman, H.W.; Steele, W.G., Jr. *Experimentation and Uncertainty Analysis for Engineers*, 2nd ed.; John Willey & Sons: New York, NY, USA, 1989.
45. Heywood, J.B. *Internal Combustion Engine Fundamentals*, 1st ed.; McGraw-Hill, Inc.: New York, NY, USA, 1988.
46. Gumus, M. A comprehensive experimental investigation of combustion and heat release characteristics of a biodiesel (hazelnut kernel oil methyl ester) fueled direct injection compression ignition engine. *Fuel* **2010**, *89*, 2802–2814. [CrossRef]
47. Hohenberg, G.F. *Advance Approaches for Heat Transfer Calculation*; Soc Automot Eng SAE Tech Pap NO 790825 19792788-98; SAE: Warrendale, PA, USA, 1979.
48. Zhang, Z.; Li, L. Investigation of in-cylinder steam injection in a turbocharged diesel engine for waste heat recovery. *Energies* **2018**, *11*, 936. [CrossRef]
49. Song, H.; Quinton, K.S.; Peng, Z.; Zhao, H.; Ladommatos, N. Effects of oxygen content of fuels on combustion and emissions of diesel engines. *Energies* **2016**, *9*, 28. [CrossRef]
50. Yusop, A.F.; Mamat, R.; Yusaf, T.; Najafi, G. Analysis of particulate matter (PM) emissions in diesel engines using palm oil biodiesel blended with diesel fuel. *Energies* **2018**, *11*, 1039. [CrossRef]
51. Sajith, V.; Sobhan, C.B.; Peterson, G.P. Experimental investigations on the effects of cerium oxide nanoparticle fuel additives on biodiesel. *Adv. Mech. Eng.* **2010**, *2010*, 1–6. [CrossRef]